On Impact and Volcanism across the Cretaceous-Paleogene Boundary

Pincelli M. Hull[1*♦], André Bornemann[2*♦], Donald Penman[1♦], Michael J. Henehan[1,3♦], Richard D. Norris[4♦†], Paul A. Wilson[5♦†], Peter Blum[6♦†], Laia Alegret[7], Sietske Batenburg[8†], Paul R. Bown[9†], Timothy J. Bralower[10], Cecile Cournede[11,12†], Alexander Deutsch[13†], Barbara Donner[14], Oliver Friedrich[15†], Sofie Jehle[16†], Hojung Kim[9†], Dick Kroon[17], Peter Lippert[18†],Dominik Loroch[13†], Iris Moebius[15,19†], Kazuyoshi Moriya[20†], Daniel J. Peppe[21], Gregory E. Ravizza[22†], Ursula Röhl[14†], Jonathan D. Schueth[23], Julio Sepúlveda[24], Philip Sexton[25†], Elizabeth Sibert[4,26,27†], Kasia K. Śliwińska[28†], Roger E. Summons[29†], Ellen Thomas[1,30], Thomas Westerhold[14†], Jessica H. Whiteside[5†], Tatsuhiko Yamaguchi[31†], James C. Zachos[32]

1 Department of Geology and Geophysics, Yale University, 210 Whitney Ave, New Haven, CT 06511, USA
2 Bundesanstalt für Geowissenschaften und Rohstoffe, Stilleweg 2, 30655 Hannover, Germany
3 GFZ German Research Centre for Geosciences, Telegrafenberg, 14473 Potsdam, Germany
4 Scripps Institution of Oceanography, University of California San Diego, 9500 Gilman Drive, La Jolla, CA 92093-0244, USA
5 National Oceanography Centre Southampton, University of Southampton, Waterfront Campus, European Way, Southampton SO14 3ZH, UK
6 International Ocean Discovery Program, Texas A&M University, 1000 Discovery Drive, College Station, TX 77845, USA
7 Departamento de Ciencias de la Tierra & Instituto Universitario de Ciencias Ambientales, Universidad Zaragoza, 50009 Zaragoza, Spain
8 Géosciences, Université de Rennes 1, Campus de Beaulieu, 35042 Rennes, France
9 Department of Earth Sciences, University College London, Gower Street, London WC1E 6BT, UK
10 Department of Geosciences, Pennsylvania State University, University Park, PA, USA
11 CEREGE, Université Aix-Marseille, Europole de l'Arbois BP 80 1, 13545 Aix en Provence, France
12 Institute for Rock Magnetism, University of Minnesota, John T. Tale Hall, 116 Church St. SE, Minneapolis, MN 55455, USA
13 Institut für Planetologie, Universität Münster, Wihelm-Klemm-St. 10, 48149 Münster, Germany
14 MARUM – Center for Marine Environmental Sciences, University of Bremen, Leobener Strasse 8, 28359 Bremen, Germany
15 Institute of Earth Sciences, Heidelberg University, Im Neuenheimer Feld 234-236, 69120 Heidelberg, Germany
16 Institut für Geophysik und Geologie, Universität Leipzig, Talstr. 35, 04103 Leipzig, Germany
17 School of Geosciences, University of Edinburgh, Edinburgh EH8 9XP, United Kingdom
18 Department of Geology & Geophysics, The University of Utah, 115 S 1460 E, Salt Lake City, UT 84112-0102, USA
19 Department of Biogeochemical Systems, Max Planck Institute for Biogeochemistry, Hans-Knöll St. 10, 07745 Jena, Germany
20 Department of Earth Sciences, Waseda University, Nishiwaseda 1-6-1, Shinjyuku-ku, Tokyo 169-8050, Japan
21 Department of Geosciences, Baylor University, One Bear Place #97354, Waco Texas 76798-7354, USA
22 Department of Geology & Geophysics, University of Hawai'I at Manoa, Honolulu, HI 96822, USA
23 ConocoPhillips Company, 925 N Eldridge Pkwy, Houston, TX 77079, USA
24 Department of Geological Sciences and Institute of Arctic and Alpine Research, University of Colorado Boulder, UCB 450, Boulder CO 830309-0450, USA
25 School of Environment, Earth & Ecosystem Sciences, The Open University, Walton Hall, Milton Keynes MK7 6AA, UK
26 Harvard Society of Fellows, Harvard University, 78 Mount Auburn Street, Cambridge, MA 02138, USA
27 Department of Earth and Planetary Sciences, Harvard University, 20 Oxford Street, Cambridge, MA 02138, USA
28 Department of Stratigraphy, Geological Survey of Denmark and Greenland (GEUS), Øster Voldgade 10, DK-1350 Copenhagen K, Denmark
29 Department of Earth, Atmospheric and Planetary Science, Massachusetts Institute of Technology, Cambridge, MA 02139, USA
30 Department of Earth and Environmental Sciences, Wesleyan University, Middletown CT 06459, USA
31 National Museum of Nature and Science, 4-1-1 Amakubo, Tsukuba, 305-0005, Japan
32 Department of Earth and Planetary Sciences, University of California Santa Cruz, CA 95064, USA

* Co-first authors (pincelli.hull@yale.edu and andre.bornemann@bgr.de)
♦ First seven authors in order of contribution, all others alphabetical
† Primary Contribution: IODP Expedition 342 K/Pg boundary investigation

1   *Abstract*

2   The cause of the end-Cretaceous mass extinction is vigorously debated due to the occurrence of a

3   very large bolide impact and flood basalt volcanism near the boundary. Disentangling their

4   relative importance is complicated by uncertainty regarding kill mechanisms and the relative

5   timing of volcanogenic outgassing, impact, and extinction. We use carbon cycle modeling and

6   paleotemperature records to constrain the timing of volcanogenic outgassing. We found support

7   for major outgassing beginning and ending distinctly prior to the impact, with only impact

8   coinciding with mass extinction and biologically amplified carbon cycle change. Our models

9   show that these extinction-related carbon cycle changes would have allowed the ocean to absorb

10   massive amounts of CO_2, thus limiting the global warming otherwise expected from post-

11   extinction volcanism.

12

13   *Introduction*

14   Sixty-six million years ago two planetary-scale disturbances occurred within less than a million

15   years of one another. An asteroid of more than 10 km in diameter collided with the Yucatan

16   Peninsula at the boundary between the Cretaceous and the Paleogene (~66 Ma), producing the

17   ~200 km wide Chicxulub impact crater (*1-4*). Impact markers at hundreds of sites globally co-

18   occur with the deposition of the Cretaceous-Paleogene (K/Pg) boundary clay and include

19   elevated abundances of siderophilic elements such as iridium, osmium, and nickel, and tektites

20   and shocked quartz (*1, 5, 6*). During the K/Pg boundary-spanning magnetochron C29r (65.688-

21   66.398 Ma, ~ 710,000 years long (*7*)), an estimated ~500,000 km$_3$ of lava flooded across much

22   of India and into the deep sea in a large igneous province (LIP) known as the Deccan Traps (*8,*

23   *9*). Deccan volcanism was, like most flood basalt eruptions (*9-11*), episodic, with flows

24   deposited in pulses throughout magnetochron C29r (*12, 13*). That both volcanism and the impact

25   event occurred within several hundred thousand years of the K/Pg extinctions is beyond

26   reasonable doubt (*5, 9, 12, 13*). However, this still leaves many aspects uncertain, including the

27   relative timing and magnitude of volcanic effects on the biosphere (*13, 14*), the potential

28   relationship between impact and volcanism (*8, 13, 15*), and whether impact or volcanism acted

29   as the sole, primary, or joint drivers of extinction (*5, 10, 16*).

30

31   The case for the Chicxulub impact as a driver of K/Pg mass extinction includes processes

32   hypothesized to operate during the days and decades following the collision. The bolide impact

33   injected an estimated >50,000 km3 of ejecta (*4*), ~ 325 Gt of sulfur and ~425 Gt CO_2 and other

34   volatiles (*17*) into the atmosphere from the marine carbonate and anhydrite target rock of the

35   Yucatan Peninsula (*5, 18*). The combined effects of an expanding impact fireball and the re-entry

36   of molten ejecta from the skies (*19*) may have raised temperatures to the point of spontaneous

37   combustion near the impactor and caused severe heat stress and even death many thousands of

38   km away from the impact site in minutes to days after impact (*20*). In the days to years that

39   followed, nitrogen and sulfur vapors reacted to form nitric and sulfuric acids and, with CO_2

40   gases, acidified the oceans (*21-23*). Finally, models and empirical evidence suggest that the

41   combination of dust and aerosols precipitated a severe impact winter in the decades post-impact

42   (*24-27*).

43

44   Impressive though these environmental effects may be, some researchers question whether the

45   Chicxulub impactor acted as the sole or main driver of the K/Pg mass extinction for three

46   primary reasons. First, no single kill mechanism appears to explain the extinction patterns:

47   acidification (*28, 29*) and primary productivity decline (*30*) (due to darkness and cold (*26*)) are

48   favored in the marine realm, whereas heat exposure and/loss of productivity (due to fires,

49   darkness and cold (*18, 26*)) are favored in the terrestrial realm (*31, 32*). Second, asteroid and

50   comet impacts occur throughout the history of life (although likely none in the last ~500 Myr of

51   the size and force of Chicxulub (*33*)), but no other mass extinction is unambiguously linked to

52   such a collision (*34*). Third, flood basalt volcanism is strongly implicated as the driver of two of

53   the greatest mass extinctions in the last half billion years (the Permian-Triassic [P/T] and

54   Triassic-Jurassic [T/J]) leading some to favor a similar role for Deccan volcanism in the K/Pg

55   mass extinction (e.g., *35*). However, most episodes of flood basalt volcanism after the T/J

56   produced no increase in extinction rates (*36*), potentially due to important Earth system changes

57   that dampened the effects of flood basalts post-P/T.

58

59   Questions regarding the role of Deccan volcanism in driving the K/Pg mass extinction arise

60   because of the relative lack of evidence for a volcanogenic driver. Despite advances in

61   chronology, the timing of the most voluminous Deccan eruptions relative to the K/Pg extinctions

62   remains unclear (e.g., ref. 8 vs. 9). Many earlier authors argued that most Deccan flood basalts

63   (>85%) were emplaced in a relatively short interval before the K/Pg, starting around the

64   C29r/C30n boundary (~66.39 Ma) and ending well before the K/Pg impact (*11, 12*). In contrast,

65   Renne et al. (*13*) and Sprain et al. (*9*) proposed that the vast majority of Deccan basalts were

66   emplaced after the impact. Schoene et al. (*8*) largely agree with the basalt flow ages of refs. 9

67   and 13, but place the K/Pg boundary higher in the lava pile (i.e., the upper part of, or above, the

68   Poladpur unit), and therefore propose major pulses of emplacement just before and just after the

69   impact (*8*).

70

71   Pre- and post-impact scenarios are debated in part because they are tied to different

72   environmental disruption scenarios. Pre-event volcanism may have acted in concert with the

73   impact to drive K/Pg extinctions (*10*), whereas post-event volcanism suggests a role for

74   volcanism in the delayed recovery of biodiversity (*13*). For the environment and life, the main

75   environmental effects of large igneous provinces are attributed to volatile release (*37-39*), not

76   lava emplacement, and the magnitude of volcanic outgassing is not necessarily linked directly to

77   the volume of erupted lava. If early eruptive phases of flood basalt volcanism have higher

78   volatile concentrations, then most volatiles could have been released before the impact, even if

79   most of the lava was emplaced afterwards (*9*).

80

81   Here we provide constraints on Deccan Trap outgassing by comparing exceptionally well-

82   resolved and temporally detailed ocean drilling and global temperature records, with five

83   modeled end-member scenarios for the timing, magnitude, and composition of outgassing (*40*).

84   These comparisons allow us to consider the relative effects of Deccan Trap outgassing and

85   bolide impact on the marine carbon cycle and biological change.

86

87   *Marine environmental record of outgassing*

88   Deccan Trap degassing released a mix of volatiles including sulfur dioxide (SO_2), chlorine (Cl)

89   and other halogens, and carbon dioxide (CO_2), with sulfur having perhaps the greatest direct

90   effect on ecosystems through acidification and pronounced global cooling (>4.5°C) (*38*). The

91   environmental effects of sulfur dioxide, however, would have been relatively short-lived (years

92   to centuries at most) and difficult to detect in slowly accumulating deep-sea sediments. In

93   contrast, the influence of CO_2 emissions should be clearly evident in marine sediments as a

94   global warming event paired with a carbon isotope anomaly (*41*). We used this diagnostic

95   fingerprint of CO_2 emissions as a proxy for the timing of potentially disruptive outgassing of

96   sulfur (and other noxious gasses) and to test which volcanic degassing scenarios are compatible

97   with the observed record.

98

99   Two dominant features are clear in our global temperature compilation (Fig. 1) (*40*). First,

100 marine and terrestrial records show a late Maastrichtian warming event of ~2°C on average

101 (Figs. S1-S16; *42, 43, 44*) in the Cretaceous part of C29r that cools back to pre-event

102 temperatures prior to the K/Pg boundary (Fig. 1). Second, the earliest Danian has temperatures

103 comparable to those in the late Maastrichtian prior to the warming event, with temperatures

104 gradually increasing to become >1°C warmer on average by ~600 kyr after the impact. Benthic

105 foraminiferal oxygen isotope records typically track changes in global mean temperatures, and

106 they show both these features (Figs. 1, 2, S13a), as do most other archives (Figs. S1-S16). The

107 two exceptions are the bulk carbonate records and fish teeth phosphate records from El Kef

108 (Figs. S10c, S11, S12), which likely do not track global temperature for extinction-related

109 reasons (*40*), thus we excluded them from the calculation of global mean temperatures.

110

111 Our multiproxy, astronomically tuned record from the North Atlantic site (*45*) has an

112 exceptionally complete Maastrichtian sequence and a mm-thick tektite layer at the K-Pg

113 boundary (Figs. 2, S17-S19). The record documents an excursion to lower values in $\delta_{13}C$ in bulk

114 sediments coincident with $\delta_{18}O$ decline (a warming indicator) as well as a decline in osmium

115 isotope values (Fig. 2, S20-S21). Similar patterns are seen in records from the South Atlantic

116 Walvis Ridge and the North Pacific Shatsky Rise (Figs. 2, S18-S19; *42, 46*). The similarity of

117 these records amongst three such widespread localities and four sites (Fig. 2), suggests that they

118 provide a remarkably complete record of magnetochron C29r. Slight temporal offsets in the

119 apparent onset and recovery from latest Maastrichtian warming (among all sites) and in early

120 Paleogene carbon isotope patterns at Shatsky Rise, due either to short unconformities and/or the

121 limitations of cyclostratigraphic age models, illustrate the current temporal uncertainties (Fig. 2).

122 Temperature and atmospheric CO_2, as reflected in both our $\delta_{18}O$ and $\delta_{13}C$ anomalies, and recent

123 boron isotope records (*23*), returned to pre-warming values in the very latest Maastrichtian. The

124   most prominent feature in the records is the dramatic decline in $\delta^{13}C$ isotopes and change in

125   sedimentary $CaCO_3$ content beginning at the K/Pg boundary (Fig. 2).

126

127   We investigated the timing of Deccan Trap outgassing by modeling the effects of CO_2 and sulfur

128   emissions on long-term global temperatures using the geochemical box model LOSCAR (Long-

129   term Ocean Sediment CArbon Reservoir v. 2.0.4) (*47*). Guided by published hypotheses for the

130   timing and volume of trap emplacement, we tested five major Deccan Trap emission scenarios

131   differing in the timing of volatile release: (i) Case 1: Leading, majority (87%) of degassing pre-

132   K/Pg boundary (after (*10*)) (ii) Case 2: 50/50, half of degassing prior to and half following the

133   K/Pg boundary (after lower estimate in (*9*)); (iii) Case 3: Punctuated, four pulses with one major

134   event just preceding the K/Pg boundary (after (*8*)), (iv) Case 4: Lagging, majority (87%) of

135   degassing post-K/Pg boundary (inverse Case 1 pre-/post- outgassing volumes, (*13*)); and (v)

136   Case 5: Spanning, emissions released evenly throughout magnetochron C29r (after (*12*)) (Table

137   1). All volcanic outgassing scenarios assume the same (i) initial climatic and oceanographic

138   conditions: 600 ppm pCO_2 and climate sensitivity of 2-4**°C** per CO_2 doubling (*41*), LOSCAR's

139   Paleogene ocean configuration and circulation, and marine $[Mg^{2+}]$ of 42 mmol/kg and $[Ca^{2+}]$ of

140   21 mmol/kg; (ii) K/Pg impact volatile release from the target rock (325 Gt S; 425 Gt CO_2)(*17*);

141   (iii) upper and lower end-estimates for total volcanic outgassing volumes (4091-9545 Gt C and

142   3200-8500 Gt S (*10*) at constant ratios) (*40*); and iv) extinction related changes in the marine

143   carbon cycle (*41, 48*) (including reductions in both organic carbon and carbonate export and

144   increases in intermediate-depth organic carbon remineralization, see Table 1) that taper back to

145   pre-event values over 1.77 Myr following the extinction (*49*). In most outgassing scenarios, we

146   assumed a common onset of Deccan degassing at the C30n/C29r boundary, following

147   geochronology of the traps (*8, 9, 12, 50*). In the GTS 2012 age framework (*7*) used to align the

148   temperature records, C30n/C29r is 358 kyr prior to the K/Pg boundary, rather than the ~250-300

149   kyrs indicated by the most recent $^{40}Ar/^{39}Ar$ and U-Pb geochronology (*8, 50*). Simulations were

150   initially tuned (*40*) to find the biological scenario (iv) that minimized data-model mismatches

151   (Figs. S22-S27) and multiple scenarios for climate sensitivity and outgassing are considered in

152   assessing goodness of fit (Figs. 3-4, S25, S28-S32, Table 2).

153

154   Three modeled scenarios differ distinctly from the observed pattern of temperature change (Fig.

155   3), thus we consider them unlikely to represent the true outgassing history. Case 3 fails to

156   reproduce the late Maastrichtian warming and shows a pronounced boundary-crossing warming

157   event that is not supported by proxy data. In Case 4, late Maastrichtian warming is too muted and

158   early Paleocene warming is too pronounced, and in Case 5 warming increases up to the K/Pg

159   boundary, unlike the empirical record (Fig. 3). Relatively poor model fit is also indicated by high

160   mean absolute errors (MAEs) for Cases 3 and 4 as compared to Cases 1 and 2 (Table 2). These

161   modeled cases also deviate considerably from the empirical $\delta_{13}C$ record (Fig 4).

162

163   Only two outgassing scenarios produce modeled temperatures resembling the empirical records:

164   the leading case (Case 1) and the 50:50 case (Case 2). We thus consider these the two most likely

165   of the tested scenarios to represent Deccan Trap outgassing. In Case 1, most CO_2 and SO_2

166   degassing occurred in the latest Maastrichtian, leading to global warming and subsequent cooling

167   prior to the K/Pg. The relatively constant early Paleocene temperatures of Case 1, with a gradual

168   warming over the 600kyrs following the impact, are also consistent with empirical records (Figs.

169   1-3, S17-S18). Case 2 (50:50) also matches the empirical temperature record well (Fig. 3), with

170   the lowest MAEs of all cases (Table 2). The Late Cretaceous warming differs between Case 1

171   and Case 2 due to the reduced Late Cretaceous volcanic outgassing in the latter. Although

172   uncertainty about climate sensitivity (*51*) and total Deccan Trap emissions (*10, 12*) has a greater

173   effect on modeled temperatures than the difference in outgassing volume (Figs. 3, S25, S28),

174   carbon isotopes also support Case 2 as the more likely scenario (Fig. 4; MAEs in Table S31).

175

176   The climatic effects of a major pulse (50%) of Deccan outgassing released over the ~350 kyr

177   immediately following the impact (Case 2) were limited by extinction-related changes to the

178   carbon cycle, including the reduction in $CaCO_3$ export from pelagic calcifiers to the seafloor.

179   Marine $CaCO_3$ export indirectly affects atmospheric CO_2 by changing the distribution of carbon

180   and alkalinity between the surface and deep-ocean, and slows the removal of alkalinity from the

181   system via $CaCO_3$ burial (*41*). The difference between Case 1 and 2 is almost imperceptible,

182   with Case 2 having slightly warmer (~0.25°C) early Danian temperatures than Case 1. Notably,

183   more rapid Paleocene outgassing, such as modeled in Case 3 (ref. 8), exceeds the capacity of the

184   altered marine carbon cycle to absorb CO_2.

185

Our results inform several important boundary debates. First, if there was a large pulse of

emplacement just 20-60 kyrs prior to the impact (*8*), most CO_2 outgassing (and associated

environmental impacts) must have preceded lava emplacement by several hundred thousand

years. This would be prior to the eruption of the most voluminous stages of Deccan volcanism

(i.e., pre-Wai subgroup) as modeled for Case 1 and 2 (Fig. 3-4; see expanded discussion in (*40*)).

Second, roughly equal pre- and post-impact volcanic degassing is supported (i.e., Case 2, Figs. 3-

4), a hypothesized scenario in ref. 9. However, our results are not consistent with most (>75%)

volcanogenic degassing post-impact (i.e., outgassing more similar to eruptive volumes in refs. *9,*

13), because modeled warming is too muted in the Cretaceous and too pronounced in the early

Paleocene (i.e., Case 4) as compared to empirical records (Fig. 3). Third, impact-related volatile

release from the target rock has a negligible climatic effect (Fig. S24), so is unlikely to account

for the dramatic warming indicated by fish teeth $\delta_{18}O$ in the first 100 kyr (*52*). Instead, this

record likely predominantly reflects changes in fish biology rather than temperature. Fourth,

biotic recovery can account for the apparently gradual early Danian warming as observed in

marine records if it begins at or shortly after impact and occurs over >1.5 myr. This biotic

recovery scenario reproduces the general pattern of change in $\delta_{13}C$ gradients (Figs. 2, S27),

carbonate saturation state (Figs. 2c, S27) and temperature, but differs from recovery hypotheses

that posit a delay in the onset of biological recovery for ~ 500kyr or more (e.g., *40, 49, 53*).

No marine evidence for joint cause in mass extinction

The fossil record indicates no lasting, outsized, or cascading effect of the late Maastrichtian

warming event on marine ecosystems of the sort that might predispose them to mass extinction

by impact. First, we found no evidence for elevated extinction rates in the latest Cretaceous in

marine taxa (Table S1), excepting a contested record from Seymour Island, Antarctica (e.g., *54,*

55). The scarcity of biostratigraphic datums in the Cretaceous portion of magnetochron C29r

signifies a conspicuous lack of extinction in widespread species including planktonic

foraminifera, nannoplankton, radiolarians, and ammonites (*7*). Second, late Cretaceous

outgassing did not have a lasting effect on the community structure of well-fossilized taxa.

Although range and community shifts coincided with warming, a shift back to the pre-warming-

like communities occurred prior to impact (see Table S1). Third, marine carbon cycle indicators

216 (δ_{13}C and carbonate deposition) show no discernable effect of late Maastrichtian outgassing and

217 warming on a major ecosystem function: the export and cycling of carbon. The δ_{13}C anomaly

218 size (~0.2-0.3 per mil; see also ref. *44*) is consistent with a volcanogenic driver as in Case 2

219 (Figs. 2, 4, S28) given the magnitude of warming, without biological amplification.

220

221 In contrast, major and enduring changes to ecosystems coincided with the K/Pg impact. In deep-

222 sea records, impact markers occur at the level of the abrupt mass extinction of >90% planktonic

223 foraminifera and 93% of nannoplankton species (Fig. 2). These groups exhibit rapid turnover and

224 high dominance in community composition in the first 500 kyrs of the Paleocene (*56, 57*), an

225 interval where bulk carbonate δ_{18}O likely reflects community composition rather than surface

226 ocean temperatures (Figs. 5, S33-S35). At the same time, tracers of the marine carbon cycle

227 indicate a profound change in marine ecosystem function. The community structure of some

228 groups such as small fishes, which show no evidence of elevated extinction, changed

229 permanently (*58*). The δ_{13}C composition of planktonic foraminifera and nannoplankton fell to or

230 below that of benthic foraminifera at the iridium anomaly (Figs. 2,5, S34-S35; *43, 49*). The loss

231 or inversion of the δ_{13}C gradient typically maintained by the biological pump is unmatched in the

232 fossil record of pelagic calcifiers (~170 million years), and indicates that the K/Pg boundary

233 impact had an outsized effect on the marine carbon cycle.

234

235 After the impact, an already altered marine carbon cycle is needed to counteract the CO_2 emitted

236 by a major post-impact pulse of outgassing as in Case 2 (Fig. 3) to avoid a warming event of the

237 same magnitude as the Late Cretaceous warming event. This suggests that the major ecological

238 change of the K/Pg mass extinction must have occurred prior to any major post-impact

239 volcanism. Our modeling does support a scenario in which Deccan volcanism could have

240 contributed to the aftermath of the impact and mass extinction as in (*13*), if environmentally

241 destructive gases such as SO_2, halogens, or sulfate aerosols contributed to (or drove) the

242 persistence of unusual marine communities for the first ~500 kyrs of the Paleocene. This might

243 be particularly true if the evolution of the magma chamber led to higher sulfur content of later

244 emissions, as in other eruption types (*59*). However, no observations document acidification

245 coupled to extreme cold snaps in the earliest Paleocene as predicted by this hypothesis, and there

246 is no explanation for why SO_2 would have greater biotic effects in the well-buffered early

247 Danian oceans than in the latest Maastrichtian oceans (Fig. S1-S18).

248

249 **Conclusion**

250 We combined climatic, biotic, and carbon cycle records with modeled impact and outgassing

251 scenarios, and found support for a bolide impact as the primary driver of the end-Cretaceous

252 mass extinction. Our analysis suggests that roughly 50% of Deccan Trap CO_2 outgassing

253 occurred well before the impact, but does not support the suggestion (*8*) that a large outgassing

254 event took place just before (~10-60 kyrs). This suggests a pronounced decoupling between CO_2

255 outgassing and lava flow emplacement if ref. 8 is correct, or a relative impact and eruption

256 chronology similar to ref. 9 and our best-supported, 50:50 outgassing scenario. The Late

257 Cretaceous warming event attributed to Deccan degassing is of a comparable size to small

258 warming events in the Paleocene and early Eocene that are not associated with elevated

259 extinction or turnover (*43, 60*), similar to what we find for the late Maastrichtian. We therefore

260 conclude that impact and extinction created the initial opportunity for the rise of Cenozoic

261 species and communities, but Deccan volcanism might have contributed to shaping them during

262 the extinction aftermath.

263

Author contributions: Among the first six authors, P.M.H conceived and co-led the study, drafted the manuscript, contributed to model design, generated empirical data, and edited data tables and figures; A.B. co-led the study and coordinated data generation, reporting, figures, and tables, generated empirical data and substantially contributed to the study design and text; D.P. led LOSCAR modeling and substantially contributed to study design and text, M.J.H. compiled and aligned age models for the global temperature compilation, prepared related tables and figures, and substantially contributed to the study design and text; R.D.N., P.A.W, and P.B. led IODP Expedition 342, with R.D.N. and P.A.W. substantially contributing to study design and text. Among the remaining co-authors, L.A., S.B., P.R.B., T.J.B., C.C., A.D., B.D., O.F., S.J., H.K., D.K., P.L., D.L., I.M., K.M., D.J.P., G.E.R., U.R., J.S., J.D.S., E.S., K.K.Ś., R.E.S., E.T., T.W., J.H.W., and T.Y. contributed empirical datasets, figures, and related analyses, interpretations and text; and L.A., P.R.B., T.J.B., O.F., D.K., P.S., J.S., E.T., T.W., J.H.W., J.C.Z. substantially contributed to ideas and/or text. All authors read and approved the final text. **Data and materials availability:** all data is available in the manuscript and the supplementary material.
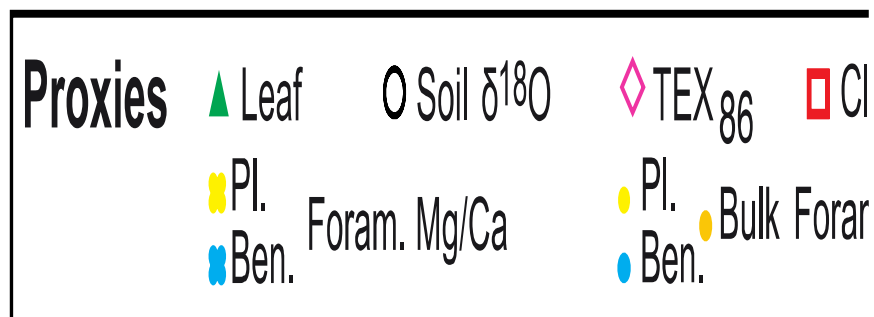
References

1. L. W. Alvarez, W. Alvarez, F. Asaro, H. V. Michel, Extraterrestrial cause for the Cretaceous-Tertiary extinction - experimental results and theoretical interpretation. *Science* **208**, 1095-1108 (1980).

2. A. R. Hildebrand *et al.*, Chicxulub crater - a possible Cretaceous Tertiary Boundary impact crater on the Yucatan Peninsula, Mexico. *Geology* **19**, 867-871 (1991).

3. B. Collen *et al.*, Clarifying misconceptions of extinction risk assessment with the IUCN Red List. *Biology Letters* **12**, 20150843 (2016).

4. J. Morgan *et al.*, Size and morphology of the Chicxulub impact crater. *Nature* **390**, 472-476 (1997).

5. P. Schulte *et al.*, The Chicxulub Asteroid Impact and Mass Extinction at the Cretaceous-Paleogene Boundary. *Science* **327**, 1214-1218 (2010).

6. G. Ravizza, D. VonderHaar, A geochemical clock in earliest Paleogene pelagic carbonates based on the impact-induced Os isotope excursion at the Cretaceous-Paleogene boundary. *Paleoceanography* **27**, PA3219 (2012).

7. F. M. Gradstein, J. G. Ogg, M. D. Schmitz, G. M. Ogg, *The Geologic Time Scale 2012*. (Elsevier B.V., Amsterdam, 2012).

8. B. Schoene *et al.*, U-Pb constraints on pulsed eruption of the Deccan Traps across the end-Cretaceous mass extinction. *Science* **363**, 862-866 (2019).

9. C. J. Sprain *et al.*, The eruptive tempo of Deccan volcanism in relation to the Cretaceous-Paleogene boundary. *Science* **363**, 866-870 (2019).

10. A. L. Chenet *et al.*, Determination of rapid Deccan eruptions across the Cretaceous-Tertiary boundary using paleomagnetic secular variation: 2. Constraints from analysis of eight new sections and synthesis for a 3500-m-thick composite section. *Journal of Geophysical Research-Solid Earth* **114**, B06103 (2009).

11. A. L. Chenet, X. Quidelleur, F. Fluteau, V. Courtillot, S. Bajpai, K-40-Ar-40 dating of the Main Deccan large igneous province: Further evidence of KTB age and short duration. *Earth and Planetary Science Letters* **263**, 1-15 (2007).

12. B. Schoene *et al.*, U-Pb geochronology of the Deccan Traps and relation to the end-Cretaceous mass extinction. *Science* **347**, 182-184 (2015).

13. P. R. Renne *et al.*, State shift in Deccan volcanism at the Cretaceous-Paleogene boundary, possibly induced by impact. *Science* **350**, 76-78 (2015).

14. P. R. Renne *et al.*, Time Scales of Critical Events Around the Cretaceous-Paleogene Boundary. *Science* **339**, 684-687 (2013).

15. M. A. Richards *et al.*, Triggering of the largest Deccan eruptions by the Chicxulub impact. *Geological Society of America Bulletin* **127**, 1507-1520 (2015).

16. E. Font *et al.*, Deccan volcanism induced high-stress environment during the Cretaceous-Paleogene transition at Zumaia, Spain: Evidence from magnetic, mineralogical and biostratigraphic records. *Earth and Planetary Science Letters* **484**, 53-66 (2018).

17. N. Artemieva, J. Morgan, E. S. Party, Quantifying the Release of Climate-Active Gases by Large Meteorite Impacts With a Case Study of Chicxulub. *Geophysical Research Letters* **44**, 10180-10188 (2017).

18. S. P. S. Gulick *et al.*, The first day of the Cenozoic. *Proceedings of the National Academy of Sciences of the United States of America* **116**, 19342-19351 (2019).

346 19. D. A. Kring, D. D. Durda, Trajectories and distribution of material ejected from the
347   Chicxulub impact crater: implications for postimpact wildfires. *Journal of Geophysical*
348   *Research-Planets* **107**, (2002).
349 20. J. Morgan, N. Artemieva, T. Goldin, Revisiting wildfires at the K-Pg boundary. *J*
350   *Geophys Res-Biogeo* **118**, 1508-1520 (2013).
351 21. S. Ohno *et al.*, Production of sulphate-rich vapour during the Chicxulub impact and
352   implications for ocean acidification. *Nature Geoscience* **7**, 279-282 (2014).
353 22. T. Tyrrell, A. Merico, D. I. A. McKay, Severity of ocean acidification following the end-
354   Cretaceous asteroid impact. *Proceedings of the National Academy of Sciences of the*
355   *United States of America* **112**, 6556-6561 (2015).
356 23. M. J. Henehan *et al.*, Rapid ocean acidification and protracted Earth System recovery
357   followed the end-Cretaceous Chixulub impact. *Proceedings of the National Academy of*
358   *Sciences of the United States of America*, (2019).
359 24. J. Vellekoop *et al.*, Rapid short-term cooling following the Chicxulub impact at the
360   Cretaceous-Paleogene boundary. *Proceedings of the National Academy of Sciences of the*
361   *United States of America* **111**, 7537-7541 (2014).
362 25. K. Kaiho *et al.*, Global climate change driven by soot at the K-Pg boundary as the cause
363   of the mass extinction. *Sci Rep-Uk* **6**, (2016).
364 26. J. Brugger, G. Feulner, S. Petri, Baby, it's cold outside: Climate model simulations of the
365   effects of the asteroid impact at the end of the Cretaceous. *Geophysical Research Letters*
366   **44**, 419-427 (2017).
367 27. C. G. Bardeen, R. R. Garcia, O. B. Toon, A. J. Conley, On transient climate change at the
368   Cretaceous-Paleogene boundary due to atmospheric soot injections. *Proceedings of the*
369   *National Academy of Sciences of the United States of America* **114**, E7415-E7424 (2017).
370 28. L. Alegret, E. Thomas, K. C. Lohmann, End-Cretaceous marine mass extinction not
371   caused by productivity collapse. *Proceedings of the National Academy of Sciences of the*
372   *United States of America* **109**, 728-732 (2012).
373 29. B. J. Marshall, R. C. Thunell, M. J. Henehan, Y. Astor, K. E. Wejnert, Planktonic
374   foraminiferal area density as a proxy for carbonate ion concentration: A calibration study
375   using the Cariaco Basin ocean time series. *Paleoceanography* **28**, 363-376 (2013).
376 30. M. Aberhan, S. Weidemeyer, W. Kiessling, R. A. Scasso, F. A. Medina, Faunal evidence
377   for reduced productivity and uncoordinated recovery in Southern Hemisphere
378   Cretaceous-Paleogene boundary sections. *Geology* **35**, 227-230 (2007).
379 31. P. M. Sheehan, T. A. Hansen, Detritus Feeding as a Buffer to Extinction at the End of the
380   Cretaceous. *Geology* **14**, 868-870 (1986).
381 32. D. S. Robertson, M. C. McKenna, O. B. Toon, S. Hope, J. A. Lillegraven, Survival in the
382   first hours of the Cenozoic. *Geological Society of America Bulletin* **116**, 760-768 (2004).
383 33. E. M. Shoemaker, Impact cratering through geologic time. *Journal of the Royal*
384   *Astronomical Society of Canada* **92**, 297-309 (1998).
385 34. J. D. Archibald *et al.*, Cretaceous Extinctions: Multiple Causes. *Science* **328**, 973-973
386   (2010).
387 35. G. Keller, J. Punekar, P. Mateo, Upheavals during the Late Maastrichtian: Volcanism,
388   climate and faunal events preceding the end-Cretaceous mass extinction.
389   *Palaeogeography Palaeoclimatology Palaeoecology* **441**, 137-151 (2016).
390 36. S. V. Sobolev *et al.*, Linking mantle plumes, large igneous provinces and environmental
391   catastrophes. *Nature* **477**, 312-U380 (2011).

392 37. M. T. Jones, D. A. Jerram, H. H. Svensen, C. Grove, The effects of large igneous
393 provinces on the global carbon and sulphur cycles. *Palaeogeography Palaeoclimatology*
394 *Palaeoecology* **441**, 4-21 (2016).
395 38. A. Schmidt *et al.*, Selective environmental stress from sulphur emitted by continental
396 flood basalt eruptions. *Nature Geoscience* **9**, 77-82 (2016).
397 39. S. Self, S. Blake, K. Sharma, M. Widdowson, S. Sephton, Sulfur and chlorine in Late
398 Cretaceous Deccan magmas and eruptive gas release. *Science* **319**, 1654-1657 (2008).
399 40. Materials and methods are available as supplementary materials at the Science website.
400 41. M. J. Henehan, P. M. Hull, D. E. Penman, J. W. B. Rae, D. N. Schmidt, Biogeochemical
401 significance of pelagic ecosystem function: an end-Cretaceous case study. *Philosophical*
402 *Transactions of the Royal Society B-Biological Sciences* **371**, 20150510 (2016).
403 42. J. S. K. Barnet *et al.*, A new high-resolution chronology for the late Maastrichtian
404 warming event: Establishing robust temporal links with the onset of Deccan volcanism.
405 *Geology* **46**, 147-150 (2018).
406 43. J. S. K. Barnet *et al.*, A high-fidelity benthic stable isotope record of Late Cretaceous-
407 Early Eocene climate change and carbon-cycling. *Paleoceanography and*
408 *Paleoclimatology* **34**, 672-691 (2019).
409 44. L. Q. Li, G. Keller, Abrupt deep-sea warming at the end of the Cretaceous. *Geology* **26**,
410 995-998 (1998).
411 45. R. D. Norris, P. A. Wilson, P. Blum, a. t. E. Scientists, in *Proc. IODP, 342,* R. D. Norris,
412 Wilson, P.A., Blum, P., and the Expedition 342 Scientists, Ed. (Integrated Ocean Drilling
413 Program, College Station, TX, 2014).
414 46. N. Robinson, G. Ravizza, R. Coccioni, B. Peucker-Ehrenbrink, R. Norris, A high-
415 resolution marine Os-187/Os-188 record for the late Maastrichtian: distinguishing the
416 chemical fingerprints of Deccan volcanism and the KP impact event. *Earth and*
417 *Planetary Science Letters* **281**, 159-168 (2009).
418 47. R. E. Zeebe, LOSCAR: Long-term Ocean-atmosphere-Sediment CArbon cycle Reservoir
419 Model v2.0.4. *Geoscientific Model Development* **5**, 149-166 (2012).
420 48. J. C. Zachos, M. A. Arthur, W. E. Dean, Geochemical evidence for suppression of
421 pelagic marine productivity at the Cretaceous/Tertiary boundary. *Nature* **337**, 61-64
422 (1989).
423 49. H. S. Birch, H. K. Coxall , P. N. Pearson, D. Kroon, D. N. Schmidt, Partial collapse of
424 the marine carbon pump after the Cretaceous-Paleogene boundary. *Geology* **44**, 287-290
425 (2016).
426 50. C. J. Sprain, P. R. Renne, W. A. Clemens, G. P. Wilson, Calibration of chron C29r: New
427 high-precision geochronologic and paleomagnetic constraints from the Hell Creek region,
428 Montana. *Geological Society of America Bulletin* **130**, 1615-1644 (2018).
429 51. E. J. Rohling *et al.*, Comparing Climate Sensitivity, Past and Present. *Annual Review of*
430 *Marine Science, Vol 10* **10**, 261-+ (2018).
431 52. K. G. MacLeod, P. C. Quinton, J. Sepulveda, M. H. Negra, Postimpact earliest Paleogene
432 warming shown by fish debris oxygen isotopes (El Kef, Tunisia). *Science* **360**, 1467-
433 1469 (2018).
434 53. S. D'Hondt, P. Donaghay, J. C. Zachos, D. Luttenberg, M. Lindinger, Organic carbon
435 fluxes and ecological recovery from the Cretaceous-Tertiary mass extinction. *Science*
436 **282**, 276-279 (1998).

437   54.   J. D. Witts *et al.*, Macrofossil evidence for a rapid and severe Cretaceous-Paleogene mass
438   extinction in Antarctica. *Nat Commun* **7**, 11738 (2016).
439   55.   T. S. Tobin, Recognition of a likely two phased extinction at the K-Pg boundary in
440   Antarctica. *Sci Rep-Uk* **7**, 16317 (2017).
441   56.   P. M. Hull, R. D. Norris, T. J. Bralower, J. D. Schueth, A role for chance in marine
442   recovery from the end-Cretaceous extinction. *Nature Geoscience* **4**, 856-860 (2011).
443   57.   J. J. Pospichal, in *The Cretaceous-Tertiary event and other catastrophes in Earth history:*
444   *Geological Society of America Special Paper 307,* G. Ryder, D. Fastovsky, S. Gartner,
445   Eds. (1996), pp. 335-360.
446   58.   E. C. Sibert, M. Friedman, P. M. Hull, G. Hunt, R. D. Norris, Two pulses of origination
447   in Pacific pelagic fish following the Cretaceous-Paleogene Mass Extinction. *Proceedings*
448   *of the Royal Society B-Biological Sciences*, 20181194 (2018).
449   59.   M. Edmonds, New geochemical insights into volcanic degassing. *Philosophical*
450   *Transactions of the Royal Society a-Mathematical Physical and Engineering Sciences*
451   **366**, 4559-4579 (2008).
452   60.   P. F. Sexton *et al.*, Eocene global warming events driven by ventilation of oceanic
453   dissolved organic carbon. *Nature* **471**, 349-352 (2011).
454   61.   R. D. Norris, in *Palaeobiology II,* D. E. G. Briggs, P. G. Crowther, Eds. (Blackwell
455   Science Ltd., Oxford, 2001), pp. 229-231.
456

457
458

Proxies ▲ Leaf   O Soil δ¹⁸O   ◇ TEX$_{86}$ □ Cl

PI.
Ben. Foram. Mg/Ca   PI.
Ben. Bulk Foram

459
460
461   **Figure 1. Global temperature change across the Cretaceous-Paleogene boundary.** New and

462   existing empirical temperature records from marine sediments (foraminiferal $\delta_{18}O$ and Mg/Ca,

463   TEX$_{86}$), shallow marine carbonates (clumped isotopes of mollusk carbonate), and terrestrial

464   proxies (leaf margin analysis, biomarkers, clumped isotopes of mollusk carbonate) were aligned

465   to common age model (Table S2 and S3) and normalized to the latest Cretaceous temperature

466   within each record. A 60pt fast Fourier transform smoother of global temperature change is

467   shown in dark red. Data are provided in Table S4-S12. Some outlying data points do not fall

468   within plot bounds, but can be seen in Figs. S1-S16.

469

470

471

472
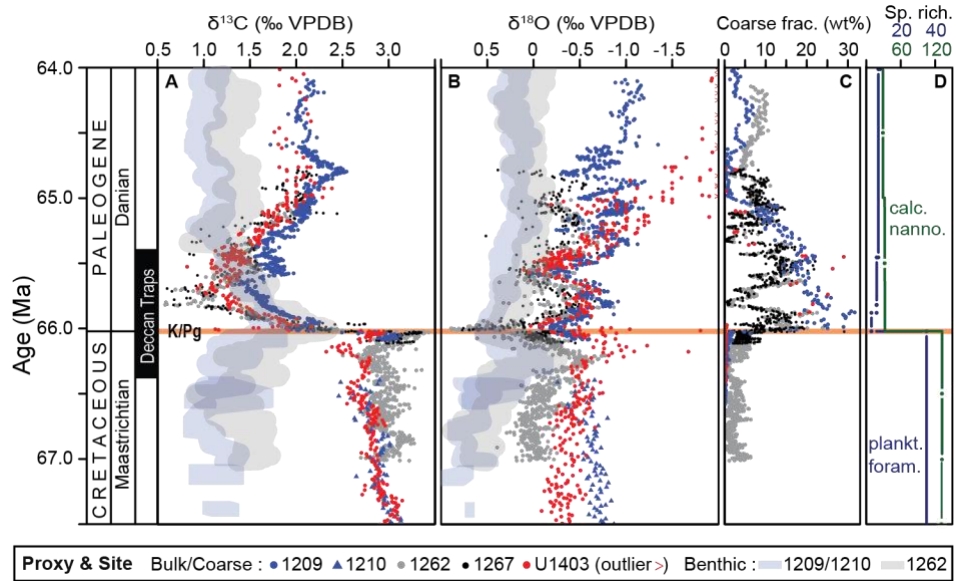
Figure 2. K/Pg boundary dynamics at the best-resolved deep-sea sites globally: Shatsky Rise, Walvis Ridge, and J-Anomaly Ridge. High resolution carbon (A) and oxygen (B) isotope dynamics in benthic foraminifera (transparent lines) and bulk carbonate (discrete points), and sediment composition (C, weight % coarse fraction), at Shatsky Rise (blue), Walvis Ridge (grey), and J-Anomaly Ridge (red), compared to (D) global records of nannofossil (grey) and foraminifera (blue, from (*61*)) species richness (*40*). Major interval of Deccan Trap emplacement (estimated 93% of volume) indicated at left by the black bar, after ref 9.

480
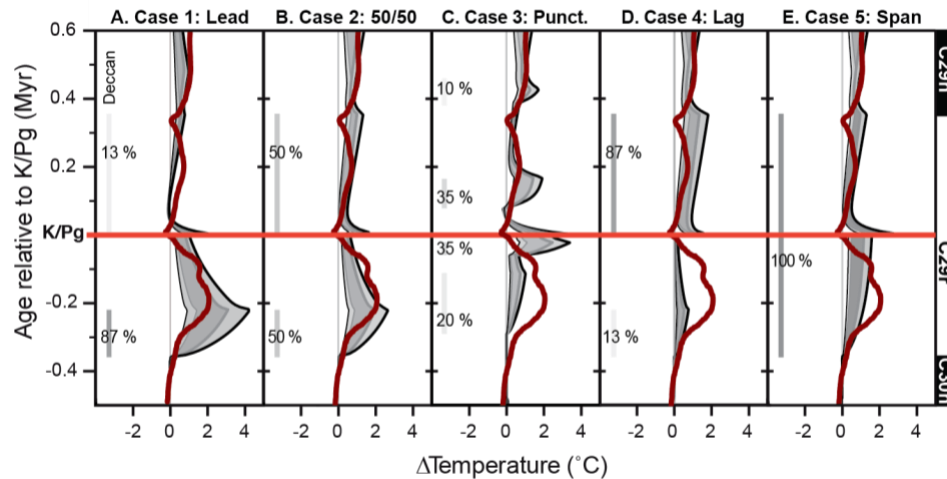
Figure 3. Global temperature change across the Cretaceous-Paleogene boundary as compared to five scenarios for Deccan Trap outgassing. Outgassing scenarios include (A) Case 1 (Leading): most outgassing prior to impact, (B) Case 2 (50/50): 50% outgassing prior to and 50% post impact, (C) Case 3 (Punctuated), (D) Case 4 (Lagging): most outgassing post impact, and (E) Case 5 (Spanning): continuous outgassing throughout magnetochron C29r (Table 1). Each model scenario is represented by four lines (bounding a shaded region) delineating different combinations of climate sensitivity and volcanic outgassing: high degassing (9545 GtC and 8500 GtS) and 3°C/doubling (thick grey line); high degassing and 4°C/doubling (thick black line); low degassing (4090 GtC and 3200 GtS) and 3°C/doubling (thin grey line), and low degassing and 2°C/doubling (thin black line), and compared to a 60pt fast Fourier transform smoother of global temperature change (red line) from Fig. 1. Deccan outgassing timing indicated by bars at left, with the shading intensity of the bar indicative of the proportion outgassing in that interval.
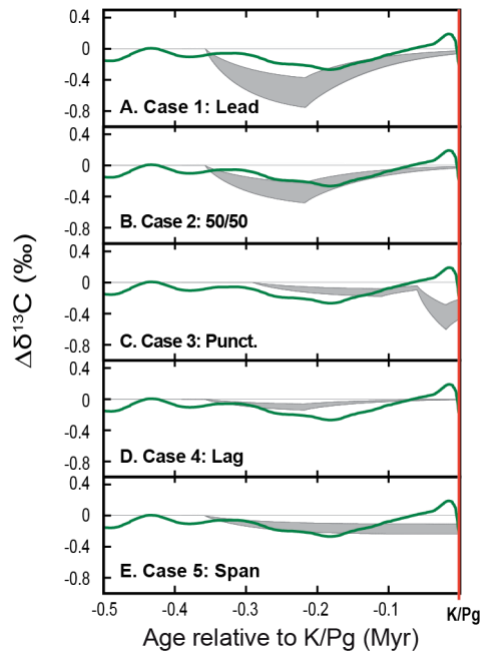
Figure 4. Surface ocean δ13C change across the late Maastrichtian warming as compared to five scenarios for Deccan Trap outgassing. Bulk carbonate $\Delta\delta13C$ (20pt fast Fourier transform smoother of Site U1403 and Site 1262 data) shown against surface ocean δ13C for end-member outgassing and climate sensitivity scenarios (grey envelope) for each case as detailed in Fig. 3. In each case, carbonate carbon isotopes are expressed as $\Delta\delta13C$, relative to the late Maastrichtian high of 3.03 ‰ at 0.432 Myr prior to the onset of the CO_2 release (see also Figs. S36-S37).
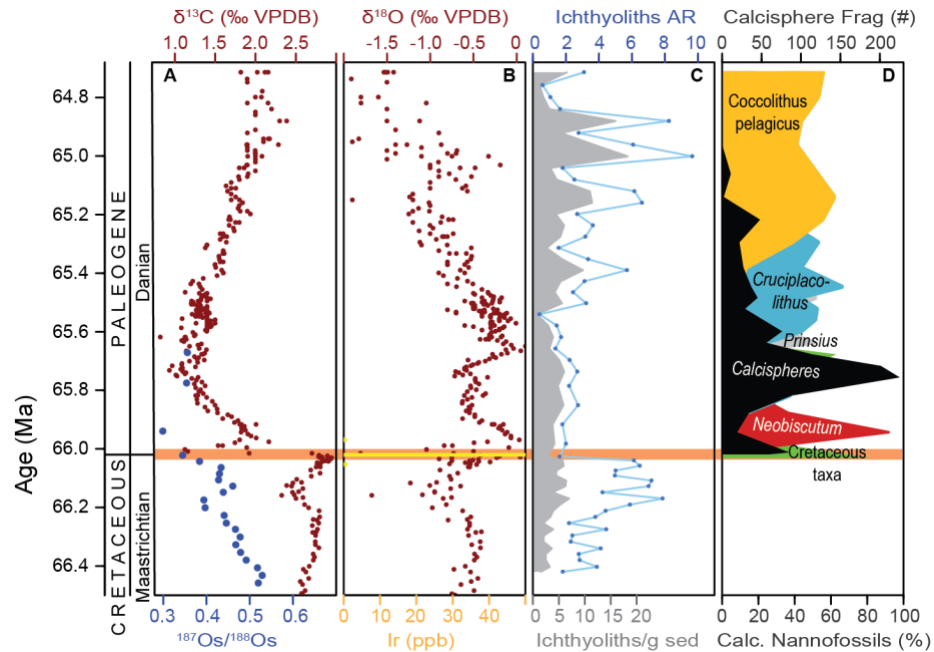
Figure 5. Late Cretaceous warming and early Paleocene record of environmental and biotic change at IODP Site U1403, J-Anomaly Ridge, Newfoundland. A negative carbon isotope anomaly (A) coincides with late Cretaceous warming in $\delta_{18}O$ (B), and osmium isotope evidence for volcanism (A) at IODP Site U1403. The collapse in surface ocean $\delta_{13}C$ values (A) coincides with iridium anomaly (B), and step change in fish tooth accumulation (C). Earliest Paleocene $\delta_{18}O$ values of bulk carbonate appear to be strongly influenced by vital effects driven by rapid turnover in the dominant calcareous nannofossil taxa (D) in sites globally (Figs. S18, S34, S35). Data in Tables S12, S16, S17, S29.

516 **Table 1. Model parameters for five focal Deccan outgassing scenarios tested in LOSCAR.**

		Case 1: Leading	Case 2: 50/50	Case 3: Punct.	Case 4: Lagging	Case 5: Spanning
Volcanic Outgassing	*Pulse 1 (Pre): Volume*	87% of total h: 8305 Gt C, 7395 Gt S l: 3559 Gt C, 2784 Gt S	50% of total high: 4773 Gt C, 4250 Gt S low: 2045 Gt C, 1600 Gt S	20% of total h: 1909 Gt C, 1700 Gt S l: 818 Gt C, 640 Gt S	13% of total high: 1241 Gt C, 1105 Gt S low: 532 Gt C, 416 Gt S	100% of total high: 9545 Gt C, 8500 Gt S low: 4091 Gt C, 3200 Gt S
	Timing	Starts: -358 kyr Ends: -218 kyr	Starts: -358 kyr Ends: -218 kyr	Starts: -290 kyr Ends: -110 kyr	Starts: -358 kyr Ends: -218 kyr	Starts: -358 kyr Ends: 355 kyr
	Pulse 2 (Pre): Volume			35% of total h: 3340 Gt C, 2975 Gt S l: 1431 Gt C, 1120 Gt S		
	Timing			Starts: -60 kyr Ends: -20 kyr		
	Pulse 1 (Post): Volume	13% of total h: 1241 Gt C, 1105 Gt S l: 532 Gt C, 416 Gt S	50% of total high: 4773 Gt C, 4250 Gt S low: 2045 Gt C, 1600 Gt S	35% of total h: 3340 Gt C, 2975 Gt S l: 1431 Gt C, 1120 Gt S	87% of total high: 8305 Gt C, 7395 Gt S low: 3559 Gt C, 2784 Gt S	
	Timing	Starts: 0 kyr Ends: 355 kyr	Starts: 0 kyr Ends: 355 kyr	Starts: 80 kyr Ends: 170 kyr	Starts: 0 kyr Ends: 355 kyr	
	Pulse 2 (Post): Volume			10% of total h: 955 Gt C, 850 Gt S l: 409 Gt C, 320 Gt S		
	Timing			Starts: 390 kyr Ends: 430 kyr		
Impact Outgas.	*Volume*	100% of total 115 Gt C, 325 Gt S	100% of total 115 Gt C, 325 Gt S	100% of total 115 Gt C, 325 Gt S	100% of total 115 Gt C, 325 Gt S	100% of total 115 Gt C, 325 Gt S
	Timing	Starts: 0 kyr Ends: 1 kyr	Starts: 0 kyr Ends: 1 kyr	Starts: 0 kyr Ends: 1 kyr	Starts: 0 kyr Ends: 1 kyr	Starts: 0 kyr Ends: 1 kyr
Biotic Change	*Organic Export Flux Δ*	50% reduction	50% reduction	50% reduction	50% reduction	50% reduction
	CaCO₃ Export Flux Δ	42.5% reduction	42.5% reduction	42.5% reduction	42.5% reduction	42.5% reduction
	Frac. Int.-depth C_{org} remin. Δ	22% increase	22% increase	22% increase	22% increase	22% increase
	Timing	Starts: 0 kyr immediately tapers Ends: 1770 kyr	Starts: 0 kyr immediately tapers Ends: 1770 kyr	Starts: 0 kyr immediately tapers Ends: 1770 kyr	Starts: 0 kyr immediately tapers Ends: 1770 kyr	Starts: 0 kyr immediately tapers Ends: 1770 kyr

517

518 **Table 2. Mean absolute error (MAE) and mean minimum absolute error (MMAE) of cases**
519 **relative to the interpolated global temperature record.** The mean minimum absolute error
520 (MMAE) was calculated for each case by determining whether the empirical data fell outside of
521 the temperature range bounded by the high and low outgassing scenarios given a climate
522 sensitivity of 3°C/CO_2 doubling, and, if so, by how much. MAEs were also calculated for each
523 outgassing volume and climate sensitivity shown in Fig. 3. MMAEs and MAEs were calculated
524 on a 20 kyr interpolated time step from 360kyr prior to 600 kyr post K/Pg. Case 2 consistently
525 has the lowest MAEs and Case 1 and 2 have the lowest MMAEs.
526

	Mean Min. Abs. Error	*High Volc., 3°C/CO_2 doub.*	*High Volc., 4°C/CO_2 doub.*	*Low Volc., 3°C/CO_2 doub*	*Low Volc., 2°C/CO_2 doub*
Case 1	0.25	0.46	0.65	0.50	0.58
Case 2	0.21	0.35	0.43	0.48	0.58
Case 3	0.45	0.59	0.65	0.58	0.64
Case 4	0.45	0.61	0.69	0.56	0.63
Case 5	0.29	0.40	0.44	0.53	0.61

527
528